JACS
JOURNAL OF THE AMERICAN CHEMICAL SOCIETY

Article

pubs.acs.org/JACS

Five Discrete Multinuclear Metal-Organic Assemblies from One Ligand: Deciphering the Effects of Different Templates

Imogen A. Riddell,[†] Yana R. Hristova,[†] Jack K. Clegg,[‡] Christopher S. Wood, Boris Breiner,[§] and Jonathan R. Nitschke*

Department of Chemistry, University of Cambridge, Lensfield Road, Cambridge CB2 1EW, U.K.

Supporting Information

ABSTRACT: A rigid organic ligand, formed through the *subcomponent self-assembly* of *p*-toluidine and 6,6′-diformyl-3,3′-bipyridine, was employed in a systematic investigation into the synergistic and competing effects of metal and anion templation. A range of discrete and polymeric metal-organic complexes were formed, many of which represent structure types that have not previously been observed and whose formation would not be predicted on taking into account solely geometric considerations. These complex structures, capable of binding multiple guests within individual binding pockets, were characterized by NMR, ESI-MS, and single-crystal X-ray diffraction. The factors that stabilize individual complexes and lead to the formation of one over another are discussed.

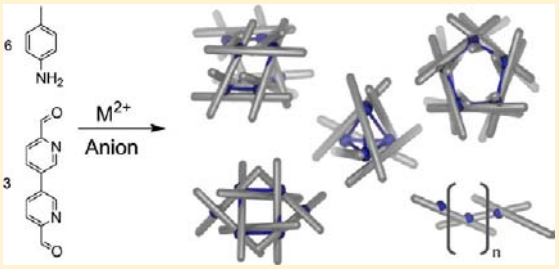

INTRODUCTION

Biological systems combine molecular components into a diverse array of supramolecular architectures, which perform the wide range of functions that underpin the processes of life.[1−6] Inspired by these natural systems, synthetic chemists have learned to use relatively simple building blocks to prepare a wide variety of high-symmetry, functional three-dimensional architectures from metal ions and ligands, including tetrahedra,[7−10] cubes,[11−13] prisms,[14−17] and spheres.[18−22]

These metal-organic polyhedra have received attention due to the unique chemical environments and well-defined void spaces of their inner cavities. The constrictive nature of the void pocket and the chemical environments found inside such complexes have so far been utilized to alter the behavior and reactivity of guest molecules,[23−26] discriminate between guest molecules,[4,11,27,28] and sequester gases.[29,30] The encapsulation abilities of these hosts allow them to add or release individual components within molecular systems,[31−38] thus changing those systems' behaviors.

New applications require the preparation of new host architectures; a promising direction involves the preparation of multicompartmental hosts,[39,40] capable of binding several guests in discrete binding pockets. Such hosts could bind different guests cooperatively[41] or modulate reactions between guest species.

The generation of such functional architectures requires fine control over self-assembly processes and a nuanced understanding of the factors that favor one structure over another. Current methods employed for the discovery of novel metal-organic assemblies focus on either geometric design principles or serendipitous discovery with retrospective structural analysis. Both methodologies highlight how subtle changes in the identity of the metal ion,[42−44] its ligands' geometries,[19,45−49] or the presence of a templating molecule or ion[50−57] can result in substantial changes in the structure of the final product. An increasingly nuanced understanding of the interplay of these different effects is thus necessary in order to prepare ever more complex targets, whose intricate structures[58−63] reflect increasingly complex functions.[4,11,23−26,29,64,65]

Studies of how the same organic building blocks can produce markedly different product structures when combined with different metal ions and anionic templates[12,66−68] are valuable because they allow for subtle templation effects to be deconvoluted. Herein we present the results of an investigation into the effects of metal-ion variation and anion templation on the formation of complex metallo-supramolecular systems.[69] Combination of the self-assembled bis-bidentate ligand **L** (Scheme 1) with the first-row divalent transition metals iron(II), cobalt(II), nickel(II), and zinc(II), together with the anions bis(trifluoromethanesulfonyl)imide (NTf_2^- or triflimide), tetrafluoroborate, trifluoromethanesulfonate (OTf^- or triflate), perchlorate, and nitrate, was explored. Only six distinct product structures were observed (Scheme 1). In each case, we observed one of four discrete products M-**1**−M-**4**, a polymeric product M-**5** or a dynamic combinatorial library (**DCL**),[70−73] a mixture of different products with none predominating. Common secondary-structure-directing factors[60] were observed to play key roles in determining the outcome of this series of self-assembly reactions.

We have previously reported the synthesis of the Fe_4L_6 tetrahedron Fe-**1**, which forms through the reaction of iron(II) with ligand **L** (generated in turn from the in situ condensation of an aniline and 6,6′-diformyl-3,3′-bipyridine) irrespective of

Received: November 22, 2012
Published: January 23, 2013

   dx.doi.org/10.1021/ja311285b | *J. Am. Chem. Soc.* 2013, 135, 2723−2733

Scheme 1. Subcomponent Self-Assembly of *p*-Toluidine, 6,6′-Diformyl-3,3′-Bipyridine, and a Range of Metal Ions (Fe^{II}, Ni^{II}, Co^{II}, Zn^{II}) and Anions (NO_3^-, BF_4^-, ClO_4^-, OTf^-, NTf_2^-) to Generate One of Six Outcomes: Discrete Complexes M-1−M-4, Polymeric Product M-5, or a DCL, Formed When No Specific Structure Is Available[a]

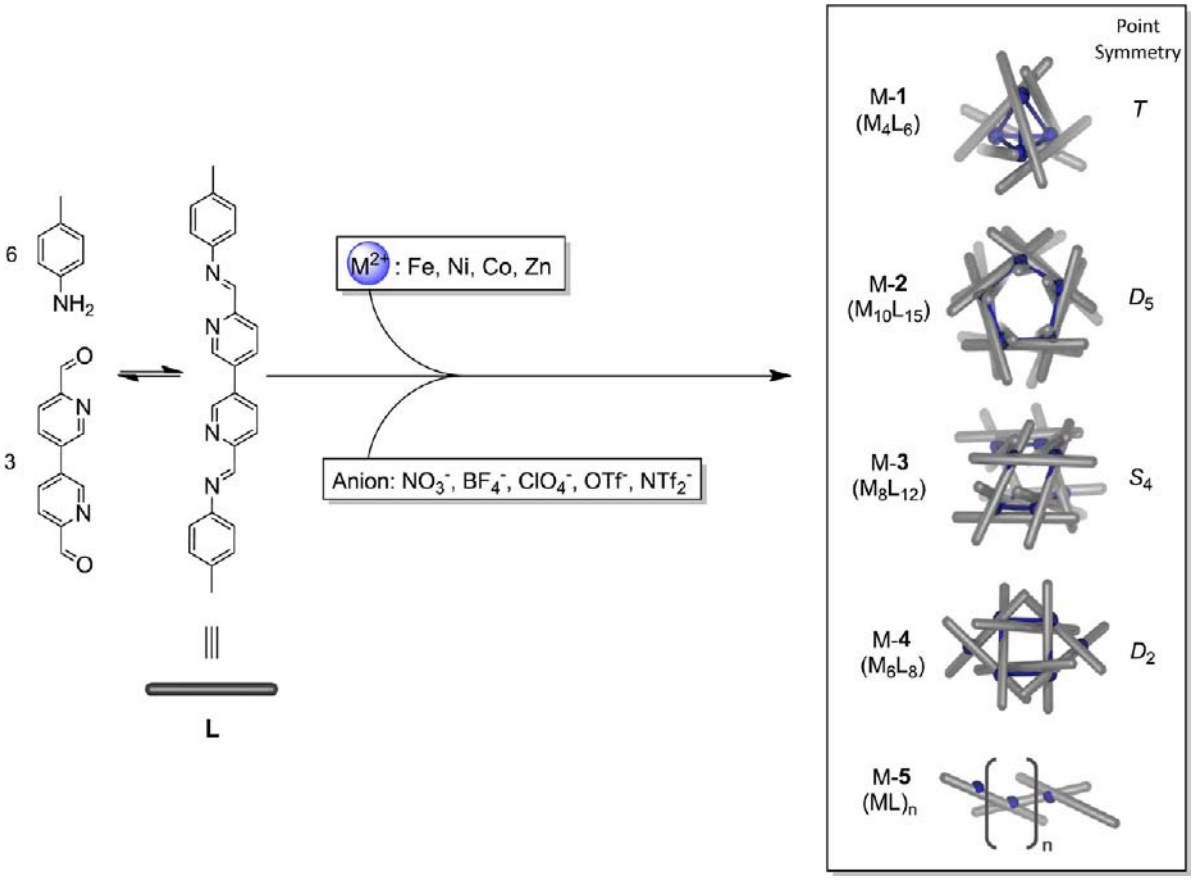

[a]Details of the structure type generated by each metal and anion combination are given in Table 1.

the choice of anion.[4,74] In contrast, we observed that when the same reaction was repeated with cobalt(II) triflimide, a dynamic library of products was formed, which collapsed upon addition of an appropriate anionic template, to form either the analogous Co_4L_6 tetrahedral cage Co-**1** or the unprecedented $Co_{10}L_{15}$ pentagonal-prismatic structure Co-**2**. The formation of Co-**2** was favored due to a combination of $\pi-\pi$ stacking, electrostatic interactions, and good space filling of the anions within the pockets they occupy.[41]

This work places these prior results into a broader and deeper context, showing how the interplay between metal ionic radius and anion size can allow the selection of a single product structure from the diverse range of architectures of Scheme 1, which often contain multiple binding pockets. Bringing these concepts together with principles of geometrical analysis[47] provides a framework for the design of assemblies even more complex than those described herein.

RESULTS AND DISCUSSION

Iron(II) Complexes. As previously reported,[4,74] the tetrahedral cage Fe-**1** was able to bind BF_4^-, OTf^-, and PF_6^- within the cavity of the cage, but not the larger NTf_2^-. This result served to confirm that an anion was not necessary as a template for the self-assembly of these structures.[4,27]

In the present investigation, we probed the reactions of *p*-toluidine and 6,6′-diformyl-3,3′-bipyridine with a range of iron(II) salts following longer reaction times than were previously studied (Scheme 2). For each of the iron(II) salts investigated, the initial subcomponent self-assembly reaction

Scheme 2. Self-Assembly of a Series of Fe_4L_6 Tetrahedral Cages, Fe-1, and $Fe_{10}L_{15}$ Pentagonal Prisms, Fe-2

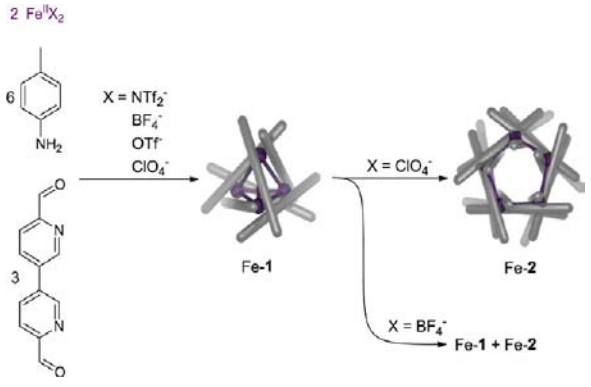

generated tetrahedral Fe-**1**. The tetrafluoroborate and perchlorate Fe-**1** complexes were shown to undergo structural rearrangement upon heating, whereby the Fe_4L_6 tetrahedra were converted into $Fe_{10}L_{15}$ pentagonal prisms, Fe-**2** (Scheme 2), with the same metal to ligand ratio.

Initial ^1H NMR and ESI-MS data for the iron(II) perchlorate reaction mixture were consistent with the formation of a

dx.doi.org/10.1021/ja311285b | J. Am. Chem. Soc. 2013, 135, 2723−2733

tetrahedral cage, Fe-**1**. The X-ray crystal structure of [ClO_4⊂Fe-**1**′] and the related tetrafluoroborate complex formed with aniline in place of *p*-toluidine, Fe-**1**′, confirmed encapsulation of an anion within the *T*-symmetric tetrahedral host molecule (Figure S13, Supporting Information).

Heating a solution of [ClO_4⊂Fe-**1**] in CD_3CN at 353 K for three days resulted in the gradual appearance of a new set of peaks in the ^{1}H NMR spectrum, which corresponded to a lower symmetry species having three nonequivalent ^{1}H NMR environments per ligand proton. ESI-MS analysis of this reaction mixture indicated the presence of a species with the formula $Fe_{10}L_{15}$, analogous to the Co-**2** species previously reported.[41] A diffusion ordered spectroscopy (DOSY) NMR experiment confirmed that the new species was larger than Fe-**1** (Figure S8, Supporting Information), with observed diffusion coefficients of $D = 1.0 \times 10^{-9}$ and 6.3×10^{-10} m^2 s^{-1} for Fe-**1** and Fe-**2**, respectively. Continued heating of the sample for 23 days resulted in the complete conversion of Fe-**1** to Fe-**2**.

Confirmation of the structure of [$Cl(ClO_4)_5$⊂Fe-**2**] was achieved through X-ray crystallographic analysis of a dark purple crystal grown though slow diffusion of diethyl ether into an acetonitrile solution of Fe-**2**. The overall architecture is barrel-like and has idealized D_5 point symmetry, resembling a twisted pentagonal prism (Figure 1a) that consists of two Fe_5L_5

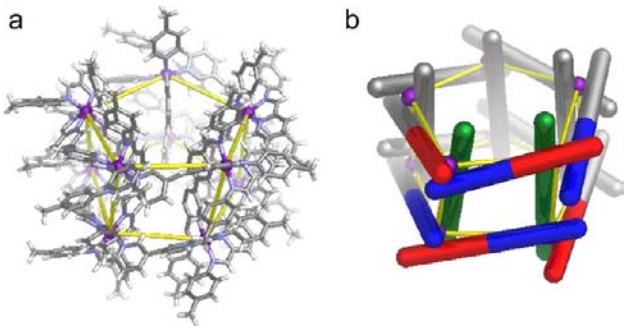

Figure 1. (a) X-ray crystal structure of pentagonal prism Fe-**2**. (b) Schematic representation of the connectivity of the ligands (different colors represent distinct ^{1}H NMR environments).

circular helicates stacked one above the other, bridged by five additional axial ligands which saturate the ten Fe^{II} coordination spheres. Unlike previously published pentagonal- and trigonal-prismatic structures,[75−77] individual ligands experience different environments within the Fe-**2** complex, with three magnetically distinct environments (Figure 1b) being observed by NMR. Extensive $\pi-\pi$ interactions between the electron-rich toluidine and electron-poor pyridine rings are inferred[41] to stabilize the structure. All of the metal centers in Fe-**2** display *meridional* (*mer*) stereochemistry.

Heating a solution of [BF_4⊂Fe-**1**]·7BF_4 at 343 K for 12 days also resulted in the conversion of Fe-**1** to Fe-**2**; however, no conditions were identified under which [BF_4⊂Fe-**1**] could be completely converted into Fe-**2**. The formation of the tetrafluoroborate adduct of Fe-**2** was confirmed by ^{1}H NMR and ESI-MS analysis.

When Fe-**1** prepared from iron(II) triflate or triflimide was heated for 13 weeks at 343 K, no evidence for their conversion to Fe-**2** was obtained, signaling the requirement for an anionic template of suitable size and shape to bring about the conversion of Fe-**1** to Fe-**2**.

Perchlorate and tetrafluoroborate are both tetrahedral and have similar volumes. Both anions can act as guests for Fe-**1** and were observed to rapidly exchange between the cavity of **1** and the solution on the NMR time scale, with BF_4^- binding less well ($K_a(BF_4^-) = 2.3 \times 10^4$ M^{-1}; $K_a(ClO_4^-) = 5.7 \times 10^5$ M^{-1}).[4] These anions were also shown to be of suitable size and shape for incorporation within the binding pockets of Fe-**2**. Taken together, the observations that ClO_4^- binds more strongly to Fe-**1** than does BF_4^- and that BF_4^- always produced a mixture of Fe-**1** and Fe-**2** in equilibrium, while ClO_4^- favored complete conversion to Fe-**2**, allow us to infer that ClO_4^- must bind with more affinity than BF_4^- within the peripheral binding pockets of Fe-**2**.

In contrast to what was observed in the case of the other metal nitrate salts investigated (see below), addition of 8 equivalents of tetrabutylammonium nitrate to [MeCN⊂Fe-**1**]·8NTf_2 gave a green precipitate and a green solution with a broad ^{1}H NMR spectrum. No discrete species could be identified by either ^{1}H NMR or ESI-MS; we attribute this outcome to the oxidation of Fe^{II} by NO_3^-.[78]

Cobalt(II) Complexes. This study follows from an initial report[41] detailing the preparation and characterization of a Co-**DCL**, the tetrahedron Co-**1**, and pentagonal prism Co-**2**. In the current work prolonged reaction times and the effects of tetrafluoroborate and nitrate anion templates were investigated. A variety of architectures were observed to form with Co^{II}, including the novel extended circular helicate structure Co-**4** and distorted cuboid Co-**3** (Scheme 3), as discussed below.

We attribute the more diverse range of architectures observed with Co^{II} in contrast to those for Fe^{II} to the greater flexibility engendered by the increased ionic radius of the high-spin d^7 cobalt(II) ion relative to the rigid geometrical requirements imposed by low-spin d^6 iron(II).[78]

The reaction of $Co(BF_4)_2 \cdot 6H_2O$ with *p*-toluidine and 6,6′-diformyl-3,3′-bipyridine resulted in the formation of two distinct products, Co-**2** and Co-**3**, in a 0.9/1 ratio, as observed by ^{1}H NMR and ESI-MS (Figures S14 and S16, Supporting Information).

ESI-MS of the new product, Co-**3**, was consistent with its formulation as Co_8L_{12} (Figure 2). The ^{1}H NMR spectrum revealed six magnetically distinct environments per ligand proton, the signals of which were well separated due to the paramagnetism of Co^{II}. Three distinct resonances are observed in the ^{19}F NMR spectrum of the as-prepared mixture of Co-**2** and Co-**3**. Two of these signals are attributed to encapsulated BF_4^- at −143.4 and −152.4 ppm, corresponding to the four tetrafluoroborates encapsulated in cuboid Co-**3** and the five in barrel Co-**2**, respectively, and a final signal at the chemical shift of free BF_4^-, observed at −145.1 ppm (Figure S15, Supporting Information).

Possible arrangements of an M_8L_{12} species, where M is hexacoordinate and **L** is bis-bidentate, include a C_{2v}-symmetric cuneane,[79] giving rise to five nonequivalent NMR environments in a 1/1/2/4/4 ratio, an S_6 slanted cube, with four nonequivalent NMR environments in a 1/1/1/1 ratio,[80] or an S_4 distorted cuboid, producing six nonequivalent NMR environments in a 1/1/1/1/1/1 ratio. Only the last is consistent with the NMR and MS data recorded. The assignment of this geometry was consistent with the X-ray structure of the analogous Ni-**3** complex (Figure 4), as discussed below. An MM2 model[81] of Co-**3** based on the crystal structure of Ni-**3** is shown in Figure 2.

dx.doi.org/10.1021/ja311285b | J. Am. Chem. Soc. 2013, 135, 2723−2733

Scheme 3. Preparation of Different Co(II)-Containing Products from Cobalt(II) Salts and the Subcomponents of Ligand L: Tetrahedron Co-1,[41] Pentagonal Prism Co-2,[41] Distorted Cuboid Co-3, and Extended Circular Helicate Co-4

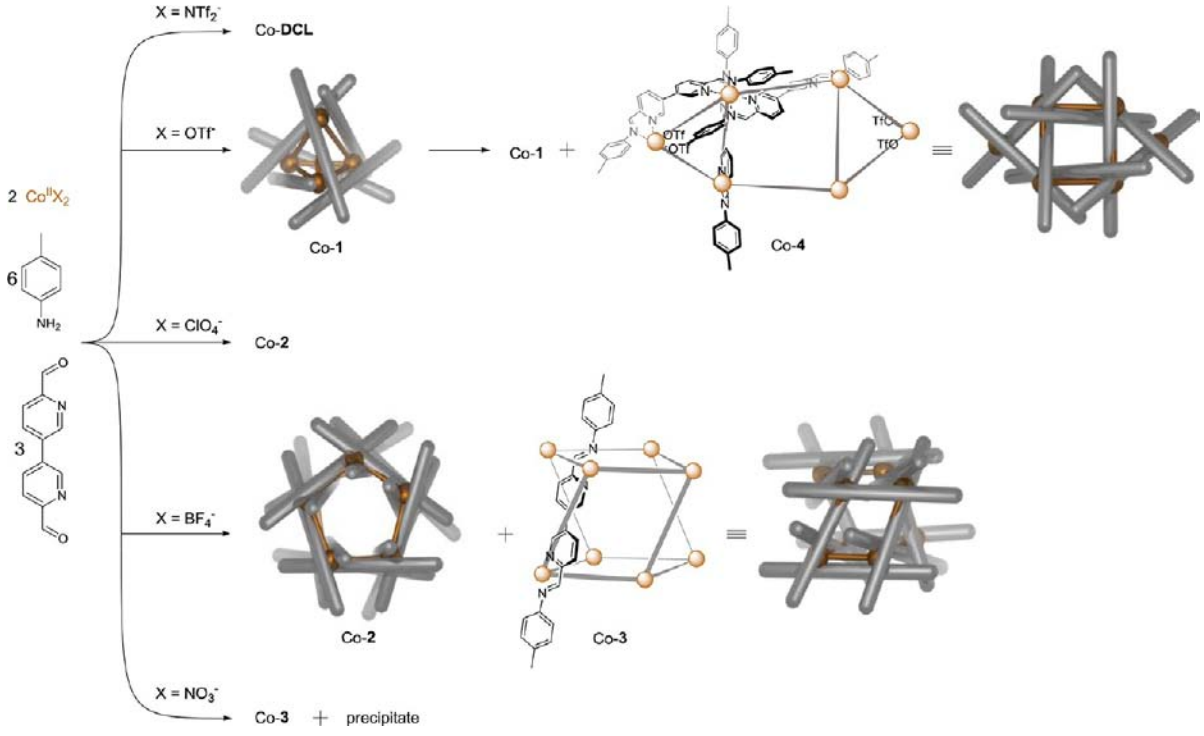

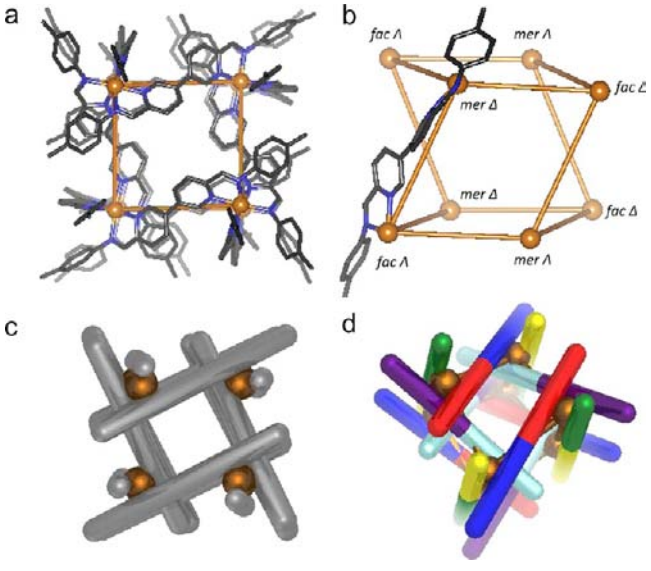

Figure 2. MM2 models of (a) distorted cuboid Co-**3**, in a view down the S_4 axis, (b) side view of Co-**3** indicating the stereochemical configuration at each metal center, (c) schematic representation of Co-**3** (rods represent **L** and orange spheres represent Co^{II} ions), and (d) a view colored to show the distinct ^1H NMR environments.

Single-crystal X-ray diffraction analysis of $[Cl(BF_4)_5 \subset$Co-**2**$]$ (Figure S17, Supporting Information) showed this structure to be analogous to the previously reported[41] M-**2** structures.

Heating the mixture of Co-**2** and Co-**3** over 14 days resulted in no observable change in the ^1H NMR spectrum. Upon crystallization Co-**2** was the sole product isolated from the reaction mixture. Upon redissolving and heating crystals of Co-**2** at 363 K for seven days, no evidence for the formation of Co-**3** was obtained. This suggests that, once formed, both products are kinetically stable with a high activation energy barrier that prevents interconversion between the two species.

The use of $Co(NO_3)_2 \cdot 6H_2O$ in the subcomponent self-assembly reaction produced a precipitate and a pale orange solution. The ^1H NMR showed six nonequivalent environments, and ESI-MS was consistent with a $Co_8\mathbf{L}_{12}$ complex, Co-**3**, analogous to that observed from $Co(BF_4)_2$.

The formation of the Co-**3** distorted cuboid in the presence of BF_4^- and NO_3^- was attributed to the decreased quality of fit for these anions within the other architectures. The individual factors governing fit are discussed below.

As previously reported,[41] a tetrahedral cage, Co-**1**, was the product isolated when $Co(OTf)_2$ was employed. However, after an acetonitrile solution of Co-**1** was heated for 50 days at 363 K, peaks corresponding to a second species were observed to grow in to the ^1H NMR spectrum, reaching a maximum integrated intensity of 0.4/1 with respect to Co-**1**. The ^1H NMR and ESI-MS data for this species were consistent with formation of an $Co_6\mathbf{L}_8$ structure, Co-**4**, analogous to Ni-**4** formed from $Ni(OTf)_2$ (discussion below; Figure 5). The ability of triflate to act both as an internal template and also as a ligand, capable of direct coordination to the metal center, resulted in the formation of this structure that deviated from the 2/3 M/**L** ratio exhibited by structure types **1**−**3**.

In addition to the anions discussed in this investigation, the formation of host−guest complexes was attempted by adding Na_2SO_4, Na_2SeO_4, Na_2TeO_4, Na_2MoO_4, $(NH_4)_2GeF_6$ or $(NH_4)_2SnF_6$ to a solution of Co-**DCL**. No evidence for encapsulation of any of these dianionic guests was observed after heating at 363 K for several days, and all of the guests with the exception of GeF_6^{2-} resulted in the formation of some precipitate.

Nickel(II) Complexes. The outcomes of the subcomponent self-assembly reactions of *p*-toluidine, 6,6′-diformyl-3,3′-bipyr-

dx.doi.org/10.1021/ja311285b | J. Am. Chem. Soc. 2013, 135, 2723−2733

idine, and the Ni^{II} salts investigated within this study are displayed in Scheme 4. As with the Co^{II} system, a suitably sized

Scheme 4. Self-Assembly of a Series of Ni^{II}-Containing Products: Ni-DCL, Tetrahedron Ni-1, Pentagonal Prism Ni-2, Cuboid Ni-3, and Extended Circular Helicate Ni-4

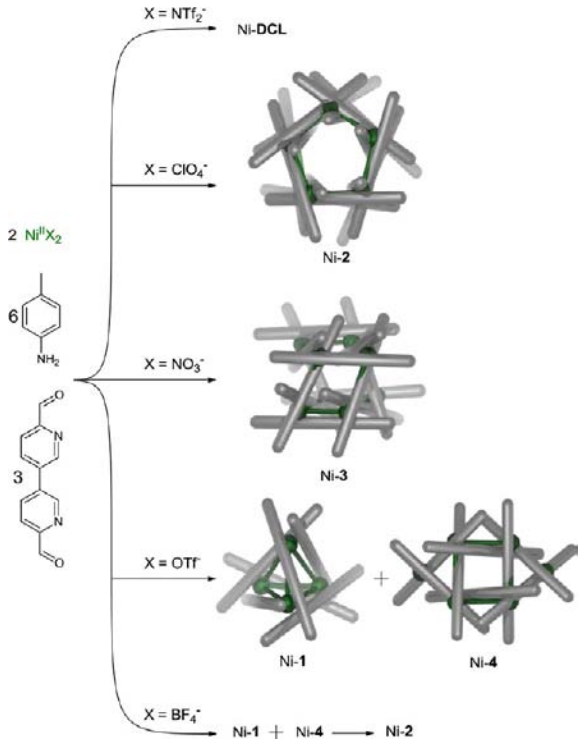

anion is necessary in order to template a discrete product; when nickel(II) triflimide was used, a collection of products was obtained whose ESI mass spectrum reflected Ni_nL_m complexes with varying stoichiometries of Ni^{II}, ligand **L**, triflimide counterions, and solvent molecules. With appropriate anionic templates, we again observed a wider variety of structures in contrast to the limited configurations adopted by Fe^{II} and **L**.

Octahedral nickel(II) has a smaller ionic radius (0.69 Å) than cobalt(II) (0.75 Å).[82] ^{1}H NMR of complexes containing octahedrally coordinated Ni^{II} produced little insight, due to the long relaxation times arising from the orbitally nondegenerate ground state of these complexes.[83,84] As a result, insight into the outcome of the self-assembly reactions was gained solely through ESI-MS and X-ray crystallography; the structures observed in each case corresponded to those of the related Fe^{II}, Co^{II}, and Zn^{II} metal-organic complexes.

Crystals of the pentagonal-prismatic product Ni-**2** were isolated following the self-assembly reaction of 6,6′-diformyl-3,3′-bipyridine, *p*-toluidine, and nickel(II) perchlorate, allowing the single-crystal X-ray structure to be solved (Figure 3). Although Ni-**2** was not observed by ESI-MS, suggesting fragility in the gas phase, when aniline was used in place of *p*-toluidine an ESI mass spectrum corresponding to an analogue of Ni-**2**, Ni-**2**′, was recorded. X-ray-quality crystals of Ni-**2**′ were also obtained, and the resulting structure (Figure S27, Supporting Information) was found to be very similar to that of Ni-**2**, sharing the pentagonal-prismatic organization of Fe-**2** and Co-**2**.

The subcomponents of **L** were observed to react with nickel(II) nitrate to give a product whose formulation as Ni-**3**, Ni_8L_{12}, (Scheme 4) was confirmed by ESI-MS and single-crystal X-ray diffraction.

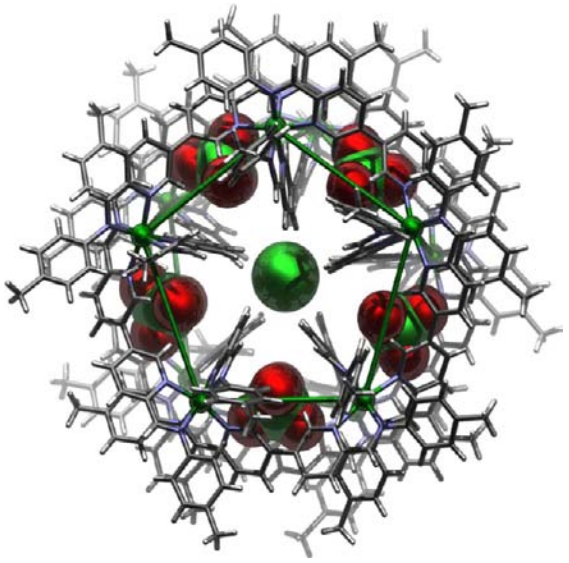

Figure 3. X-ray crystal structure of $[Cl(ClO_4)_5 \subset Ni\text{-}2]$ formed from *p*-toluidine. Solvent molecules and additional anions are omitted for clarity.

Ni-**3** has idealized S_4 point symmetry and can be described as a distorted cuboid. When they are viewed down the pseudo-S_4 axis (Figure 4a), the square faces appear to be planar with one metal center at each vertex. These "squares" are not planar, however, but puckered, as shown in Figure 4c. In contrast to the M-**2** architecture, the "axial" ligands, parallel to the principal symmetry axis (S_4 in M-**3**; C_5 in M-**2**) bridge from the top to

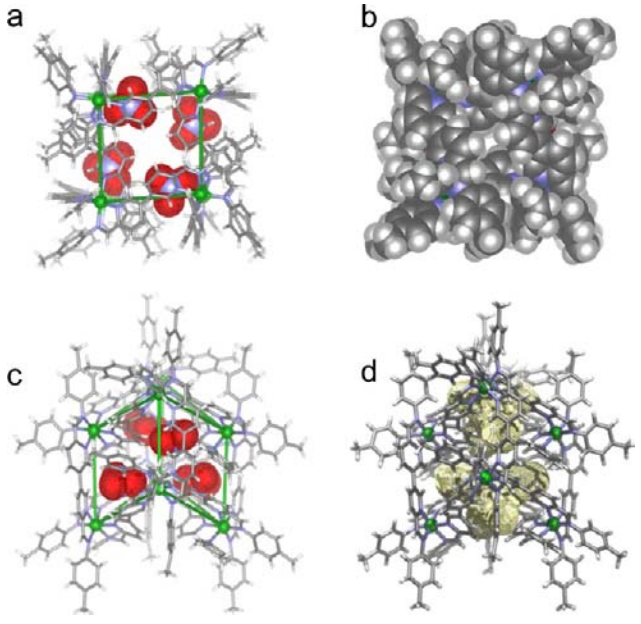

Figure 4. X-ray crystal structure of Ni-**3** with four encapsulated nitrate anions: (a) view down the S_4 axis (ball-and-stick representation); (b) space-filling model of the same view; (c) side view showing the deviation of the structure from a regular cube (green lines connect the metal centers to show the distorted cuboid geometry of the complex); (d) view showing the two distinct anion binding pockets (shaded mesh) within Ni-**3**.

dx.doi.org/10.1021/ja311285b | *J. Am. Chem. Soc.* 2013, 135, 2723−2733

the bottom of the structure on the outside, giving rise to the six discrete ligand environments observed by ^{1}H NMR in the case of Co-**3** (Figure 2d). Unlike tetrahedral Ni-**1** (having all *fac* metal centers) or pentagonal prism Ni-**2** (having all *mer* metal centers), the metal centers in Ni-**3** alternate between *fac* and *mer* conformations, resulting in four *fac* and four *mer* centers per structure. Within each "square", the two *fac* and the two *mer* centers have the same handedness (either Λ or Δ) and the opposite handedness to their closest neighbors.

This structure is closed off well with no significant openings on the sides, suggesting that the four encapsulated nitrate anions could not easily diffuse out. VOIDOO calculations (detailed in the Supporting Information) identified two discrete binding pockets of 155 Å^3, each of which contained two nitrate anions (Figure 4a,c,d and Figure S41b,c (Supporting Information)).

The saddle shape of the anion binding pockets within M-**3** ensures that only the smallest anions in this study (BF_4^- and NO_3^-) are able to fit. Once encapsulated, the anions benefit from stabilizing nonclassical H-bonding interactions with the surrounding phenylene hydrogens[85,86] and Coulombic interactions with the cationic metal centers.[41]

Nickel(II) triflate reacted with the subcomponents of **L** to yield a mixture of tetrahedron Ni-**1** and the unprecedented Ni_6L_8 extended circular helicate structure Ni-**4**. Heating the reaction mixture of Ni-**1** and Ni-**4** for ten weeks at 363 K resulted in no change in the ESI mass spectrum. X-ray diffraction analysis of a crystal grown from diffusion of diisopropyl ether into the reaction mixture revealed a structure consistent with the Ni_6L_8 composition observed by ESI-MS (Figure 5) and the ^{1}H spectrum observed for Co-**4** (discussed above).

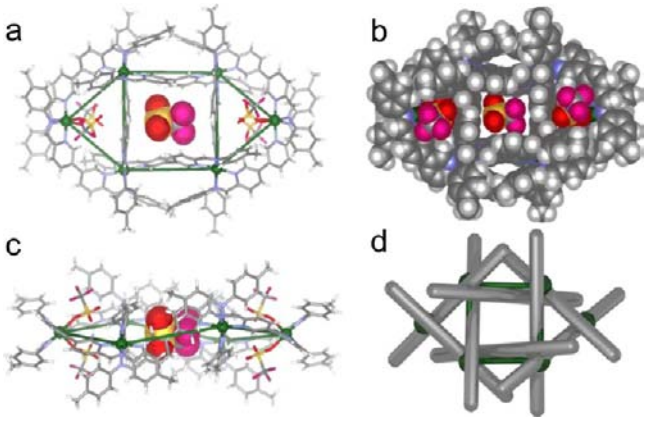

Figure 5. X-ray crystal structure of the extended circular helicate [OTf⊂Ni-**4**], with two triflate anions coordinated to each terminal Ni^{II} center and one triflate in the central void: (a) view down the C_2 axis through the center of the circular helicate core; (b) space-filling representation; (c) side view along another C_2 axis showing the twist of the structure and its deviation from planarity; (d) schematic view of the metal and ligand arrangement.

Ni-**4** has two distinct metal environments: the central four metal ions are *meridionally* bound to three bidentate pyridyl-imine fragments, while the remaining two centers are each coordinated to two pyridyl-imine groups and two monodentate triflate anions. Two distinct types of binding sites are present: two peripheral pockets, each occupied by two nickel-bound triflate anions, and a central pocket that encapsulated a single disordered triflate, which is stabilized by Coulombic and anion−π interactions.[85−87] Both kinds of binding sites are accessible via two large pores above and below the mean plane of the complex, leading to rapid triflate exchange in Co-**4** and Zn-**4**, as observed by ^{19}F NMR (described below).

The structure has idealized D_2 symmetry and can be described as an extended circular helicate, composed of a central [2 × 2] helicate unit[88,89] consisting of four ligands each adopting an *anti* conformation that bridge four metal centers, with an average metal−metal separation of 9.93 Å. Two additional triflate-coordinated nickel ions form triangular sides that extend from the central [2 × 2] helicate, with a shorter metal−metal distance of 7.84 Å (Figure 5). The six nickel(II) ions are observed to undergo a "ruffling" distortion from their mean plane (Figure 5c).

The triflate salt of Ni-**1** was also characterized by single-crystal diffraction (Figure 6) from a crystal grown by the

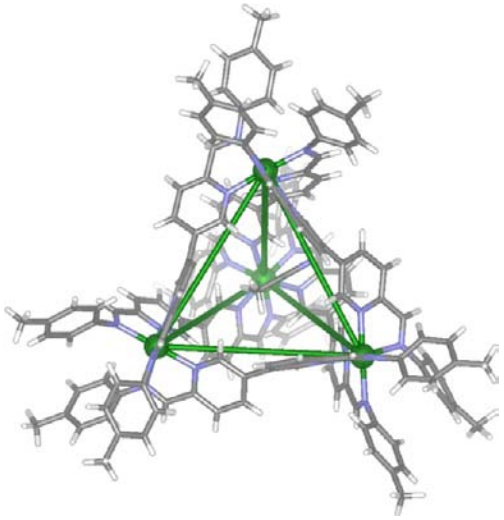

Figure 6. X-ray structure of [MeCN⊂Ni-**1**]. Solvent and counterions are omitted for clarity.

diffusion of diethyl ether into the reaction mixture described above. The structure of Ni-**1** is similar to that of Co-**1**,[41] with an acetonitrile molecule encapsulated within the central cavity rather than an anion, as observed in the case of Fe-**1**.[4] The metal-to-metal distance of Ni-**1** was measured to be 9.7 Å, intermediate between the M−M distances for Fe-**1** and Co-**1** (9.5 and 9.8 Å, respectively) and in keeping with the intermediacy of nickel(II)'s ionic radius (0.69 Å)[82] between those of Fe^{II} and Co^{II}.

The formation of a mixture of Ni-**1** and Ni-**4** highlights the versatility of this system. The Ni-**1** complex contains an appropriately sized and shaped pocket for encapsulation of the triflate anion, indicated by the anion's ability to template this structural type.[4,41] The triflate anion is, however, also coordinating enough to act as a viable ligand to the metal centers, templating the formation of Ni-**4**.

The reaction of the subcomponents of **L** with nickel(II) tetrafluoroborate in acetonitrile at 323 K yielded three products by ESI-MS. Initially the Ni-**1** tetrahedron and Ni-**4** extended circular helicate were observed; however, after heating to 363 K for two months only the Ni-**2** pentagonal prism was observed, suggesting that Ni-**2** is the thermodynamically favored nickel(II) complex in the presence of tetrafluoroborate template anions.

Zinc(II) Complexes. As with Co^{II} and Ni^{II}, the larger ionic radius of Zn^{II}, relative to that of Fe^{II}, facilitated the formation of a variety of structures in the presence of appropriate templating anions (Scheme 5). Although we observed evidence for the formation of Zn-**2**, Zn-**3**, and Zn-**4**, no evidence was observed for the formation of the Zn-**1** tetrahedron. The use of $Zn(NO_3)_2$ yielded a polymeric structure, Zn-**5**, which was unique within the scope of this investigation.

Scheme 5. Subcomponent Self-Assembly of a Series of Zn^{II}-Containing Products: Zn-DCL, Pentagonal Prism Zn-2, Cuboid Zn-3, Extended Circular Helicate Zn-4, and Polymer Zn-5

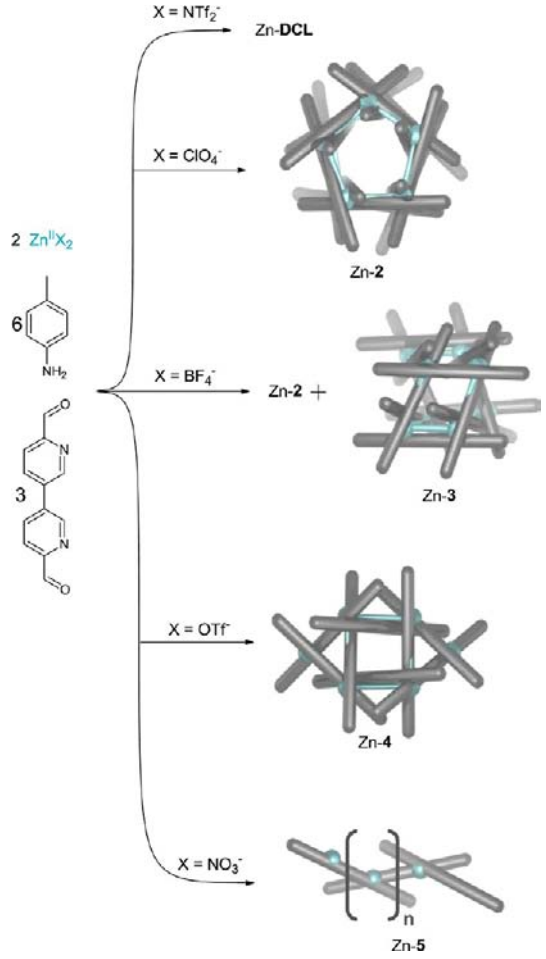

Zinc(II) has fast ligand exchange kinetics that reflect weaker metal−ligand bonds,[78] necessitating the use of ESI-MS ionization cone voltages (6 vs 18−25 eV) lower than with the other metal complexes of this study. These fast kinetics ensured rapid equilibration of reaction mixtures, while the thermodynamic lability of the system resulted in incomplete consumption of the subcomponents and formation of by-products in many cases, as noted below.

The importance of anionic templation was again evident upon reaction of the subcomponents of **L** and zinc(II) triflimide, which yielded a dynamic library of species, Zn-**DCL**, whose ESI mass spectrum reflected Zn_nL_m complexes with varying stoichiometries of Zn^{II}, ligand **L**, triflimide counterions, and solvent molecules and which possessed a correspondingly broad and complex ^{1}H NMR spectrum (Figure S29, Supporting Information).

Analysis of the reaction of $Zn(ClO_4)_2$ with the subcomponents of **L** was performed for both the crude reaction mixture and purified crystalline material. In each case the ^{1}H NMR (Figure S37, Supporting Information) revealed minor peaks in addition to those corresponding to Zn-**2**. Due to the low concentration of the minor species no corresponding signals could be observed in the ^{13}C NMR spectrum; however, peaks corresponding to species with a $Zn_{12}L_{12}$·6MeCN and $Zn_{14}L_{14}$ ratio were observed by ESI-MS alongside those corresponding to Zn-**2**. These peaks might derive from the fragmentation of a polymeric structure similar to Zn-**5**, described below.

The appearance of minor products in the case of $Zn(ClO_4)_2$ contrasted with the cases of the other metals studied; M-**2** was observed to form cleanly from the perchlorates of iron(II), cobalt(II), and nickel(II), reflecting the strong templation role of perchlorate for pentagonal-prismatic structure type **2** and the weaker ability of Zn^{II} to template imine bonds.

The reaction of zinc(II) tetrafluoroborate with 6,6′-diformyl-3,3′-bipyridine and *p*-toluidine yielded a mixture of products corresponding to $Zn_{10}L_{15}$ and Zn_8L_{12} species by ESI-MS. The ^{1}H NMR spectrum of the mixture was consistent with an attribution of these two species to Zn-**2** and Zn-**3** in a 1/0.2 ratio. The ^{1}H NMR spectrum of Zn-**3** revealed six distinct environments for each proton in a 1/1/1/1/1/1 ratio, in agreement with the solid-state observations of Ni-**3** and the ^{1}H spectrum of Co-**3**. As with Co^{II}, the ^{19}F NMR spectrum further supported this assignment, yielding three distinct signals: two signals attributed to encapsulated BF_4^- at −144.3 and −155.9 ppm, assigned to Zn-**3** and Zn-**2**, respectively, and a final signal at the chemical shift of free BF_4^-, observed at −151.4 ppm. Heating the reaction mixture of Zn-**2** and Zn-**3** at 353 K for 15 days resulted in no change in the ^{1}H NMR profile.

Following the reaction of zinc(II) triflate with the subcomponents of **L**, a Zn_6L_8 species was observed by ESI-MS. The ^{1}H NMR spectrum of this product revealed four nonequivalent environments per ligand proton in a 1/1/1/1 ratio, consistent with the product Zn-**4**, having a solution structure similar to the crystal structure of Ni-**4** (Figure 5). A single peak was observed in the ^{19}F NMR spectrum, consistent with the fast exchange of bound and free triflate anions expected for Zn-**4** and with the spectrum recorded for Co-**4**.

In contrast with the other metals studied, Zn-**1** was never observed with any of the anions of this study. From the data amassed thus far, we would expect OTf^- to be the most viable template for a Zn-**1** complex. Our failure to observe Zn-**1** when $Zn(OTf)_2$ was used leads us to infer that the stabilization energy gained upon templation of Zn-**1** does not outweigh the preference of Zn^{II} for direct ligation to triflate, generating Zn-**4**.

The reaction of zinc(II) nitrate with the subcomponents of **L** in acetonitrile resulted in the formation of an insoluble material. When the reaction was performed in methanol, the same reagents reacted to form single crystals of polymer Zn-**5** (Figure 7), with the general formula $\{[ZnL(NO_3)_2]\cdot 3CH_3OH\}_n$.

Zn-**5** consists of a one-dimensional helical coordination polymer with a repeating unit of $ZnL(NO_3)_2$. One full turn of a helical chain of Zn-**5** is composed of three repeating units, *i*, *i* + 1, and *i* + 2, where the next unit, *i* + 3, is identical to the *i*th unit. All Zn^{II} centers are octahedrally coordinated, where four of the six coordination sites are occupied by two bidentate pyridylimine moieties and the remaining two sites are occupied by nitrate anions acting as monodentate ligands (Figure 7a). In the X-ray crystal structure of polymeric Zn-**5**, the remaining

dx.doi.org/10.1021/ja311285b | J. Am. Chem. Soc. 2013, 135, 2723−2733

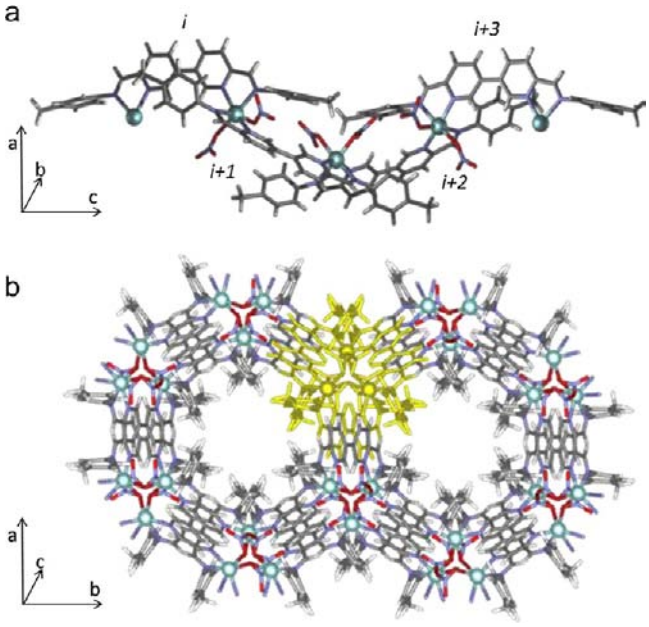

Figure 7. X-ray crystal structure of Zn-**5** with two bidentate **L** ligands and two nitrate anions coordinated to each Zn^{II} center: (a) side view along the one-dimensional polymeric helical chain showing one full turn of the helix from the *i*th to the *i* + 3rd unit; (b) view down the cavity of the channels, which consist of six helical polymeric strands stabilized by C−H···ONO_2^- interactions between coordinated nitrates and aromatic protons on a neighboring chain. The portion colored in yellow corresponds to the section of polymer shown in (a).

two oxygen atoms of the nitrates are observed to participate in nonclassical H-bonding with phenylene hydrogen atoms of ligands belonging to neighboring helical polymer strands, stabilizing the overall structure and promoting polymer formation as opposed to a discrete closed structure. Zn-**5** thus contrasts with the formation of discrete Zn-**4**, observed in the case of triflate, which is less coordinating and a less able H-bond acceptor than nitrate.

These nonclassical interactions hold six polymer strands together in a circular fashion, thus forming channels that run the length of the crystal, as shown in Figure 7b. Zn-**5** thus includes a substantial void volume, which consists of extended cylindrical pores with diameters of 8.8 Å. The volume of these pores corresponds to approximately 52% of the total volume of the unit cell in the crystal structure of Zn-**5**.[90] This significant solvent-accessible void volume is reminiscent of volumes observed in metal-organic frameworks (MOFs).[91−94]

In an attempt to evaluate the effect of the charge of the anion on the final structure, similarly to the dianions investigated with Co^{II}, K_2CrO_4 was added to Zn-**DCL**. This resulted in significant precipitate formation, and no evidence was observed for the formation of a host−guest complex.

Analysis of Structure-Directing Influences. Table 1 summarizes the different products obtained from the reactions of the subcomponents of **L** with the different metal ions and anions of this study. These results collectively suggest that the thermodynamics of formation of each structural type **1**−**5** are finely balanced. Subtle effects are able to tip this balance; changes in metal−ligand bond lengths and anion templation effects play a role in favoring the overall thermodynamic stability of one structure over another.[95]

Rearrangement of Fe-**1** into pentagonal prism Fe-**2**—the only other architecture observed to form in the case of Fe^{II}—

Table 1. Summary of the Structures Observed from the Combination of Ligand L with Different Metals and Anions[c]

Metal (Ionic Radius[83] / Å) \ Anion (Volume[28] / Å³)	NTf_2^- (156)	OTf^- (85)	ClO_4^- (55)	BF_4^- (53)	NO_3^- (41)
Fe^{II} (0.61)	**1**	**1**	[**1**] **2**	**1** **2**	[a]
Ni^{II} (0.69)	DCL	**1** **4**	**2**	[**1**] [**4**] **2**	**3**
Zn^{II} (0.74)	DCL	**4**	**2**	**2** **3**	**5**[b]
Co^{II} (0.75)	DCL	**1** **4**	**2**	**2** **3**	**3**[a]

[a]Precipitation was observed. [b]MeOD solvent. [c]The numbers shown refer to the structure types cited above: **1**, M_4L_6; **2**, $M_{10}L_{15}$; **3**, M_8L_{12}; **4**, M_6L_8; **5**, polymeric $ZnL(NO_3)_2$. Kinetic products, indicated by brackets, are completely consumed upon formation of the thermodynamic product. The table is colored according to the final equilibrated product mixture.

was only observed when a counteranion of optimal size and shape (ClO_4^- or BF_4^-) for the peripheral binding pockets of Fe-**2** was present during the self-assembly process. We infer the high kinetic barrier observed for conversion of Fe-**1** to Fe-**2** to be due to the large number of bonds which must rearrange during this transformation. The tight coordination sphere and short, strong N→Fe bonds of the iron(II) system reduces the overall kinetic lability of these systems.

The factors which result in the stabilization of pentagonal prism **2**, as noted above, include (1) optimal fit of the anions within the pockets they occupy, together with possible stabilizing anion−π interactions,[96] (2) the electrostatic interaction between each anion and the four positively charged metal ions which surround it, and (3) the enthalpic gain from favorable $\pi-\pi$ interactions between the electron-rich toluidine residues and the electron-poor pyridine residues on the equatorial ligands.

Prior investigations of the mononuclear iron and cobalt tris(*N*-phenylpyridinaldimine) complexes showed an increased preference for Co^{II} to adopt a *mer* stereochemistry of the pyridylimine ligands about the metal center, relative to the Fe^{II} analogue. Under the same conditions the Fe^{II} complex formed a 3/1 statistical mixture of *mer* and *fac* isomers, whereas Co^{II} favored *mer* coordination over the odds, exhibiting an 6/1 ratio of *mer* to *fac*.[41] We infer that this decreased tendency of Fe^{II} to adopt a *mer* coordination of the ligands around the metal center further disfavors formation of Fe-**2** and thereby increases the probability of observing the Fe-**1** structural type.

The observation that iron(II), the least versatile of the metals investigated, formed pentagonal prism **2** with ClO_4^- and BF_4^- underscores the suitability of these anions as templates for this

dx.doi.org/10.1021/ja311285b | J. Am. Chem. Soc. 2013, 135, 2723−2733

structure. This suitability is further confirmed by the observation that, across the range of metals in this study, the $M_{10}L_{15}$ structure was always observed when these anions were employed. We attribute this observation to an optimal size and shape match between the anion and the pocket it occupies and the anions' poor coordinating ability. The observation that every metal perchlorate salt exclusively formed **2**, whereas BF_4^- was observed to template other structures as well, suggests that the subtle increase in size from BF_4^- to ClO_4^- is significant, with the perchlorate anion providing a more optimal fit for the pockets within the $M_{10}L_{15}$ complex.

When M-**1** and M-**2** are no longer optimal encapsulants for a given anion, an alternative arrangement of ligands self-assembles to form a suitable host structure. In the cases of Co^{II} and Zn^{II}, complex **3** was observed to form alongside **2** in the presence of BF_4^-. Nitrate, the smallest of the anions investigated, also formed complex **3** with Ni^{II} and Co^{II}. The crystal structure of Ni-**3** showed that the binding pockets within this structure, though larger in volume than those of Ni-**2**, are an awkward saddle shape, such that only the smallest of the anions investigated could be accommodated. Complex **3**, like complex **2**, is a tightly packed structure stabilized through multiple $\pi-\pi$ interactions and the filling of its central void spaces by templating counterions. The ratio of encapsulated anions to cationic metal centers is 1/2 in both **2** and **3**, suggesting that both structures benefit from a similar degree of Coulombic stabilization.

We observed triflate to behave differently from the other anions investigated, because, like nitrate, it is able to act not only as an internal template but also as a competent O donor. This ability is manifested in the Ni-**4** extended circular helicate structure, where the terminal metal centers were each coordinated by four nitrogen donors and two triflate anions. Furthermore, the larger size and nonspherical shape of the triflate anion render it a poor fit for the pockets of complexes **2** and **3**. For Ni-**1** and Fe-**1**, triflate adducts may be formed as the binding pocket within **1** can accommodate the triflate anion. Similarly, with $Co(OTf)_2$ the M_4L_6 tetrahedron Co-**1** was observed to predominate; however, a small proportion of Co-**4** was observed at equilibrium alongside Co-**1**, which we infer to be due to the coordinating ability of the anion.

Zinc(II), the most labile of the metals examined during this study, did not exhibit the same degree of selectivity for N donors over O donors as the other metals. This resulted in formation of Zn-**4** and Zn-**5** as the major products with the OTf^- and NO_3^- anions, respectively.

CONCLUSIONS

A diverse series of anion-templated polynuclear architectures was prepared from a single self-assembled ligand. These structures included M_4L_6 tetrahedra, M_6L_8 extended circular helicates, M_8L_{12} distorted cuboids, and $M_{10}L_{15}$ pentagonal prisms. Analysis of the different factors that govern the formation of each of these structures has been carried out and the competing effects of anions and metals dissected, revealing a set of subtle rules for self-assembly. This work complements the established use of geometric design principles to predict the outcome of metal-organic self-assembly reactions,[47,97,98] by showing how secondary interactions may overrule the primary geometric design principles.[12,41,42,99] When designing metallo-supramolecular architectures, the following considerations may allow for finer-grained control over architecture.

Larger Metals Enhance Architectural Diversity. When the ionic radius is increased from Fe^{II} through Ni^{II} to Co^{II} and Zn^{II}, ligands gain freedom to link together in a greater number of ways. Metals with smaller ionic radii, such as Fe^{II}, have less adaptable coordination spheres and therefore fewer ligand conformations available to them without a severe energetic cost. The subtle increase in freedom engendered by the more flexible ligand arrangement around a larger metal center, reflected in the low energetic cost to small deviations of a coordination sphere from an ideal coordination geometry, facilitate significant structural diversification.

Subtle Differences in the Size of the Anions Have a Large Impact on the Structure. Despite the similarity in sizes of the polyatomic anions investigated herein, a diverse range of architectures were formed, ranging from well-studied M_4L_6 tetrahedra through to more complex multianion-templated $M_{10}L_{15}$ or M_8L_{12} structures to the unprecedented M_6L_8 extended circular helicate and helical metallo-polymer Zn-**5**. A good fit between the size and shape of an anionic template and the corresponding binding pocket was a necessary precondition for the formation of the structures described herein.

Both *fac* and *mer* Coordination of Ligands around a Metal Center Must Be Considered. Ward's work[42,67,99] provides good examples in which *mer* stereochemistry led to the formation of intricate and complex structures with flexible ligands;[100] here we show how even rigid ligands can generate complex architectures through linking metal centers of different stereochemical configurations. In this study, the combination of all *fac* vertices within a single structure gives rise to exclusively the M_4L_6 tetrahedron **1**, as would be predicted using classical geometric design principles.[47,97,98] However, inclusion of *mer* vertices within a structure allows for the new architectures **2**–**4** to be created. The ratio of *mer* to *fac* isomers may be altered through choice of an appropriate metal ion[41] or ligand design,[101,102] providing a further means to control the outcome of such complex self-assembling systems.

The use of these principles has allowed us to understand the outcomes of the present study and sets clear directions for exploration of larger, more complex multicompartmental architectures and the new functions that they promise.

EXPERIMENTAL SECTION

General Procedure for Metal Complex Synthesis. Stoichiometric quantities of transition-metal salt (2 equiv), 6,6′-diformyl-3,3′-bipyridine (3 equiv), and *p*-toluidine (6 equiv) were loaded into a J. Young NMR tube/Schlenk flask and dissolved in acetonitrile. The reaction vessel was subjected to three evacuation/nitrogen fill cycles to remove oxygen, sealed, and then heated for several days at an appropriate temperature. Zn-**5** was prepared in CD_3OD because insoluble, amorphous products were observed to precipitate from CD_3CN. Individual complexes could be isolated by precipitation or crystallization upon addition of either diethyl ether or diisopropyl ether. Specific details are provided in the Supporting Information

ASSOCIATED CONTENT

Supporting Information

Text, figures, and CIF files giving full characterization data, including experimental procedures, NMR and ESI-MS spectra, details of the calculation of the volumes, and crystallographic data. This material is available free of charge via the Internet at http://pubs.acs.org. Crystallographic data have also been deposited with the CCDC (file nos. 893781–893790).

AUTHOR INFORMATION

Corresponding Author

E-mail: jrn34@cam.ac.uk.

Present Addresses

[‡]School of Chemistry and Molecular Biosciences, The University of Queensland, Brisbane St Lucia, QLD, Australia 4072.

[§]Base4 Innovation, Broers Building, JJ Thompson Avenue, Cambridge CB3 0FA, U.K.

Author Contributions

[†]These authors contributed equally to this work.

Funding

This work was supported by the U.K. Engineering and Physical Sciences Research Council (EPSRC) (I.A.R. and J.R.N.), the Cambridge European Trust (Y.R.H.), the Marie Curie IIF scheme of the seventh EU Framework Program (J.K.C.), and the Isaac Newton Trust (B.B.).

Notes

The authors declare no competing financial interest.

ACKNOWLEDGMENTS

We thank the EPSRC Mass Spectrometry Service at Swansea, the National Crystallography Service at Southampton for collecting X-ray data, P. Grice and D. Howe for help with NMR experiments, C. Sporikou for the synthesis of 6,6′-diformyl-3,3′-bipyridine, and Dr. A. Stefankiewicz, Dr. G. D. Pantoş, and Dr. M. M. J. Smulders for helpful discussions. We thank the Diamond Light Source (UK) for synchrotron beam time on I19 (MT6791 and MT7114).

REFERENCES

(1) Umena, Y.; Kawakami, K.; Shen, J.-R.; Kamiya, N. *Nature* **2011**, *473*, 55.
(2) Katen, S.; Zlotnick, A. *Methods Enzymol.* **2009**, *455*, 395.
(3) Lehn, J.-M.; Rigault, A. *Angew. Chem., Int. Ed.* **1988**, *27*, 1095.
(4) Hristova, Y. R.; Smulders, M. M. J.; Clegg, J. K.; Breiner, B.; Nitschke, J. R. *Chem. Sci.* **2011**, *2*, 638.
(5) Crichton, R. R.; Declercq, J.-P. *Biochim. Biophys. Acta, Gen. Subj.* **2010**, *1800*, 706.
(6) Fornasari, M. S.; Laplagne, D. A.; Frankel, N.; Cauerhff, A. A.; Goldbaum, F. A.; Echave, J. *Mol. Biol. Evol.* **2004**, *21*, 97.
(7) Bilbeisi, R. A.; Clegg, J. K.; Elgrishi, N.; Hatten, X. d.; Devillard, M.; Breiner, B.; Mal, P.; Nitschke, J. R. *J. Am. Chem. Soc.* **2011**, *134*, 5110.
(8) Meng, W.; Clegg, J. K.; Thoburn, J. D.; Nitschke, J. R. *J. Am. Chem. Soc.* **2011**, *133*, 13652.
(9) Liu, T.; Liu, Y.; Xuan, W.; Cui, Y. *Angew. Chem., Int. Ed.* **2010**, *49*, 4121.
(10) Glasson, C. R. K.; Meehan, G. V.; Motti, C. A.; Clegg, J. K.; Turner, P.; Jensen, P.; Lindoy, L. F. *Dalton Trans.* **2011**, *40*, 10481.
(11) Meng, W.; Breiner, B.; Rissanen, K.; Thoburn, J. D.; Clegg, J. K.; Nitschke, J. R. *Angew. Chem., Int. Ed.* **2011**, *50*, 3479.
(12) Tidmarsh, I. S.; Faust, T. B.; Adams, H.; Harding, L. P.; Russo, L.; Clegg, W.; Ward, M. D. *J. Am. Chem. Soc.* **2008**, *130*, 15167.
(13) Alkordi, M. H.; Belof, J. L.; Rivera, E.; Wojtas, L.; Eddaoudi, M. *Chem. Sci.* **2011**, *2*, 1695.
(14) Zhao, Z.; Zheng, Y.-R.; Wang, M.; Pollock, J. B.; Stang, P. J. *Inorg. Chem.* **2010**, *49*, 8653.
(15) Lusby, P. J.; Muller, P.; Pike, S. J.; Slawin, A. M. Z. *J. Am. Chem. Soc.* **2009**, *131*, 16398.
(16) Fan, J.; Saha, M. L.; Song, B.; Schonherr, H.; Schmittel, M. *J. Am. Chem. Soc.* **2012**, *134*, 150.
(17) Vacek, J.; Caskey, D. C.; Horinek, D.; Shoemaker, R. K.; Stang, P. J.; Michl, J. *J. Am. Chem. Soc.* **2008**, *130*, 7629.
(18) Stephenson, A.; Argent, S. P.; Riis-Johannessen, T.; Tidmarsh, I. S.; Ward, M. D. *J. Am. Chem. Soc.* **2011**, *133*, 858.
(19) Sun, Q.-F.; Iwasa, J.; Ogawa, D.; Ishido, Y.; Sato, S.; Ozeki, T.; Sei, Y.; Yamaguchi, K.; Fujita, M. *Science* **2010**, *328*, 1144.
(20) Jin, P.; Dalgarno, S. J.; Atwood, J. L. *Coord. Chem. Rev.* **2010**, *254*, 1760.
(21) Bai, J.; Virovets, A. V.; Scheer, M. *Science* **2003**, *300*, 781.
(22) Sun, Q.-F.; Sato, S.; Fujita, M. *Nat. Chem.* **2012**, *4*, 330.
(23) Yoshizawa, M.; Klosterman, J. K.; Fujita, M. *Angew. Chem., Int. Ed.* **2009**, *48*, 3418.
(24) Breiner, B.; Clegg, J. K.; Nitschke, J. R. *Chem. Sci.* **2011**, *2*, 51.
(25) Pluth, M. D.; Bergman, R. G.; Raymond, K. N. *Acc. Chem. Res.* **2009**, *42*, 1650.
(26) Smulders, M. M. J.; Nitschke, J. R. *Chem. Sci.* **2012**, *3*, 785.
(27) Glasson, C. R. K.; Meehan, G. V.; Clegg, J. K.; Lindoy, L. F.; Turner, P.; Duriska, M. B.; Willis, R. *Chem. Commun.* **2008**, 1190.
(28) Clegg, J. K.; Cremers, J.; Hogben, A. J.; Breiner, B.; Smulders, M. M. J.; Thoburn, J. D.; Nitschke, J. R. *Chem. Sci.* **2013**, *4*, 68.
(29) Riddell, I. A.; Smulders, M. M. J.; Clegg, J. K.; Nitschke, J. R. *Chem. Commun.* **2011**, *47*, 457.
(30) Duriska, M. B.; Neville, S. M.; Lu, J.; Iremonger, S. S.; Boas, J. F.; Kepert, C. J.; Batten, S. R. *Angew. Chem., Int. Ed.* **2009**, *48*, 8919.
(31) Ludlow, R. F.; Otto, S. *Chem. Soc. Rev.* **2008**, *37*, 101.
(32) Osowska, K.; Miljanić, O. S. *Synlett* **2011**, 1643.
(33) Zheng, Y.-R.; Yang, H.-B.; Ghosh, K.; Zhao, L.; Stang, P. *Chem. Eur. J.* **2009**, *15*, 7203.
(34) Dadon, Z.; Wagner, N.; Ashkenasy, G. *Angew. Chem., Int. Ed.* **2008**, *47*, 6128.
(35) Allen, V. C.; Robertson, C. C.; Turega, S. M.; Philp, D. *Org. Lett.* **2010**, *12*, 1920.
(36) Nitschke, J. R. *Nature* **2009**, *462*, 736.
(37) Chung, M.-K.; Severin, K.; Lee, S. J.; Waters, M. L.; Gagne, M. R. *Chem. Sci.* **2011**, *2*, 744.
(38) Ray, D.; Foy, J. T.; Hughes, R. P.; Aprahamian, I. *Nat. Chem.* **2012**, *4*, 757.
(39) Baxter, P. N. W.; Lehn, J.-M.; Kneisel, B. O.; Baum, G.; Fenske, D. *Chem. Eur. J.* **1999**, *5*, 113.
(40) Freye, S.; Hey, J.; Torras-Galán, A.; Stalke, D.; Herbst-Irmer, R.; John, M.; Clever, G. H. *Angew. Chem., Int. Ed.* **2012**, *51*, 2191.
(41) Riddell, I. A.; Smulders, M. M. J.; Clegg, J. K.; Hristova, Y. R.; Breiner, B.; Thoburn, J. D.; Nitschke, J. R. *Nat. Chem.* **2012**, *4*, 751.
(42) Ward, M. D. *Chem. Commun.* **2009**, 4487.
(43) Pentecost, C. D.; Chichak, K. S.; Peters, A. J.; Cave, G. W. V.; Stoddart, J. F.; Cantrill, S. J. *Angew. Chem., Int. Ed.* **2007**, *46*, 218.
(44) Johnson, A. M.; Moshe, O.; Gamboa, A. S.; Langloss, B. W.; Limtiaco, J. F. K.; Larive, C. K.; Hooley, R. J. *Inorg. Chem.* **2011**, *50*, 9430.
(45) Lehn, J. M. *Supramolecular Chemistry: Concepts and Perspectives*; Wiley-VCH: Weinheim, Germany, 1995.
(46) Glasson, C. R. K.; Lindoy, L. F.; Meehan, G. V. *Coord. Chem. Rev.* **2008**, *252*, 940.
(47) Caulder, D. L.; Raymond, K. N. *Acc. Chem. Res.* **1999**, *32*, 975.
(48) Saalfrank, R. W.; Maid, H.; Scheurer, A. *Angew. Chem., Int. Ed.* **2008**, *47*, 8794.
(49) Chakrabarty, R.; Mukherjee, P. S.; Stang, P. J. *Chem. Rev.* **2011**, *111*, 6810.
(50) Hasenknopf, B.; Lehn, J. M.; Kneisel, B. O.; Baum, G.; Fenske, D. *Angew. Chem., Int. Ed.* **1996**, *35*, 1838.
(51) Busch, D. H. *Science* **1971**, *171*, 241.
(52) Lankshear, M. D.; Beer, P. D. *Coord. Chem. Rev.* **2006**, *250*, 3142.
(53) Gong, H.-Y.; Rambo, B. M.; Cho, W.; Lynch, V. M.; Oh, M.; Sessler, J. L. *Chem. Commun.* **2011**, *47*, 5973.
(54) Scherer, M.; Caulder, D. L.; Johnson, D. W.; Raymond, K. N. *Angew. Chem., Int. Ed.* **1999**, *38*, 1588.
(55) Dry, E. F. V.; Clegg, J. K.; Breiner, B.; Whitaker, D. E.; Stefak, R.; Nitschke, J. R. *Chem. Commun.* **2011**, *47*, 6021.

(56) O'Sullivan, M. C.; Sprafke, J. K.; Kondratuk, D. V.; Rinfray, C.; Claridge, T. D. W.; Saywell, A.; Blunt, M. O.; O'Shea, J. N.; Beton, P. H.; Malfois, M.; Anderson, H. L. *Nature* **2011**, *469*, 72.
(57) Custelcean, R.; Bonnesen, P. V.; Duncan, N. C.; Zhang, X.; Watson, L. A.; Van Berkel, G.; Parson, W. B.; Hay, B. P. *J. Am. Chem. Soc.* **2012**, *134*, 8525.
(58) Ayme, J.-F.; Beves, J. E.; Leigh, D. A.; McBurney, R. T.; Rissanen, K.; Schultz, D. *Nat. Chem.* **2012**, *4*, 15.
(59) Cantrill, S. J.; Chichak, K. S.; Peters, A. J.; Stoddart, J. F. *Acc. Chem. Res.* **2005**, *38*, 1.
(60) Smulders, M. M. J.; Riddell, I. A.; Browne, C.; Nitschke, J. R. *Chem. Soc. Rev.* **2013**, *42*, 1728.
(61) Piguet, C.; Borkovec, M.; Hamacek, J.; Zeckert, K. *Coord. Chem. Rev.* **2005**, *247*, 705.
(62) Hamacek, J.; Borkovec, M.; Piguet, C. *Dalton Trans.* **2006**, 1473.
(63) Santoni, M.-P.; Pal, A. K.; Hanan, G. S.; Tang, M.-C.; Venne, K.; Furtos, A.; Menard-Tremblay, P.; Malveau, C.; Hasenknopf, B. *Chem. Commun.* **2012**, *48*, 200.
(64) de Hatten, X.; Asil, D.; Friend, R. H.; Nitschke, J. R. *J. Am. Chem. Soc.* **2012**, *134*, 19170.
(65) de Hatten, X.; Bell, N.; Yufa, N.; Christmann, G.; Nitschke, J. R. *J. Am. Chem. Soc.* **2011**, *133*, 3158.
(66) Giles, I. D.; Chifotides, H. T.; Shatruk, M.; Dunbar, K. R. *Chem. Commun.* **2011**, *47*, 12604.
(67) Najar, A. M.; Tidmarsh, I. S.; Adams, H.; Ward, M. D. *Inorg. Chem.* **2009**, *48*, 11871.
(68) Duriska, M. B.; Neville, S. M.; Lu, J.; Iremonger, S. S.; Boas, J. F.; Kepert, C. J.; Batten, S. R. *Angew. Chem., Int. Ed.* **2009**, *48*, 8919.
(69) Pluth, M. D.; Johnson, D. W.; Szigethy, G.; Davis, A. V.; Teat, S. J.; Oliver, A. G.; Bergman, R. G.; Raymond, K. N. *Inorg. Chem.* **2009**, *48*, 111.
(70) Leclaire, J.; Vial, L.; Otto, S.; Sanders, J. K. M. *Chem. Commun.* **2005**, 1959.
(71) Corbett, P. T.; Leclaire, J.; Vial, L.; West, K. R.; Wietor, J.-L.; Sanders, J. K. M.; Otto, S. *Chem. Rev.* **2006**, *106*, 3652.
(72) Otto, S.; Furlan, R. L. E.; Sanders, J. K. M. *Science* **2002**, *297*, 590.
(73) Lam, R. T. S.; Belenguer, A.; Roberts, S. L.; Naumann, C.; Jarrosson, T.; Otto, S.; Sanders, J. K. M. *Science* **2005**, *308*, 667.
(74) Ousaka, N.; Clegg, J. K.; Nitschke, J. R. *Angew. Chem., Int. Ed.* **2012**, *51*, 1464.
(75) Bar, A. K.; Chakrabarty, R.; Mostafa, G.; Mukherjee, P. S. *Angew. Chem., Int. Ed.* **2008**, *47*, 8455.
(76) Bar, A. K.; Mohapatra, S.; Zangrando, E.; Mukherjee, P. S. *Chem. Eur. J.* **2012**, *18*, 9571.
(77) Fujita, N.; Biradha, K.; Fujita, M.; Sakamoto, S.; Yamaguchi, K. *Angew. Chem., Int. Ed.* **2001**, *40*, 1718.
(78) Cotton, F. A.; Wilkinson, G.; Murillo, C. A.; Bochmann, M. *Advanced Inorganic Chemistry*, 6th ed.; Wiley: Hoboken, NJ, 1999.
(79) Stephenson, A.; Ward, M. D. *Dalton Trans.* **2011**, *40*, 7824.
(80) Bell, Z. R.; Harding, L. P.; Ward, M. D. *Chem. Commun.* **2003**, 2432.
(81) *Cache Version 7.5.0.85 ed.*; Fujitsu Limited, 2000−2006.
(82) Greenwood, N. N.; Earnshaw, A. *Chemistry of the Elements*; Pergamon: Oxford, U.K., 1985.
(83) *Current Methods in Inorganic Chemistry*; Ivono Bertini, C. L., Giacomo, P., Eds.; Elsevier: Amsterdam, 2001; Vol. 2, p 75.
(84) *Current Methods in Inorganic Chemistry*; Ivono Bertini, C. L., Giacomo, P., Eds.; Elsevier: Amsterdam, 2001; Vol. 2, p 143.
(85) Constable, E. C.; Redondo, A. H.; Housecroft, C. E.; Neuburger, M.; Schaffner, S. *Dalton Trans.* **2009**, 6634.
(86) Mandel-Gutfreund, Y.; Margalit, H.; Jernigan, R. L.; Zhurkin, V. B. *J. Mol. Biol.* **1998**, *277*, 1129.
(87) Nobukuni, H.; Shimazaki, Y.; Tani, F.; Naruta, Y. *Angew. Chem., Int. Ed.* **2007**, *46*, 8975.
(88) Nitschke, J. R.; Hutin, M.; Bernardinelli, G. *Angew. Chem., Int. Ed.* **2004**, *43*, 6724.
(89) Campbell, V. E.; Nitschke, J. R. *Synlett* **2008**, 3077.
(90) Spek, A. L. *PLATON: A multipurpose Crystallographic Tool*, Utrecht University: Utrecht, The Netherlands, 2008.
(91) An, J.; Farha, O. K.; Hupp, J. T.; Pohl, E.; Yeh, J. I.; Rosi, N. L. *Nat. Commun.* **2012**, *3*, 604.
(92) Murray, L. J.; Dinca, M.; Long, J. R. *Chem. Soc. Rev.* **2009**, *38*, 1294.
(93) Yaghi, O. M.; Li, H.; Davis, C.; Richardson, D.; Groy, T. L. *Acc. Chem. Res.* **1998**, *31*, 474.
(94) Li, H.; Eddaoudi, M.; O'Keeffe, M.; Yaghi, O. M. *Nature* **1999**, *402*, 276.
(95) Brooker, S.; Lan, Y.; Price, J. R. *Dalton Trans.* **2007**, 1807.
(96) Schottel, B. L.; Chifotides, H. T.; Dunbar, K. R. *Chem. Soc. Rev.* **2008**, *37*, 68.
(97) Stang, P. J.; Olenyuk, B. *Acc. Chem. Res.* **1997**, *30*, 502.
(98) Tranchemontagne, D. J.; Ni, Z.; O'Keeffe, M.; Yaghi, O. M. *Angew. Chem., Int. Ed.* **2008**, *47*, 5136.
(99) Stephenson, A.; Ward, M. D. *Dalton Trans.* **2011**, *40*, 7824.
(100) Ayme, J.-F.; Beves, J. E.; Leigh, D. A.; McBurney, R. T.; Rissanen, K.; Schultz, D. *J. Am. Chem. Soc.* **2012**, *134*, 9488.
(101) Howson, S. E.; Allan, L. E. N.; Chmel, N. P.; Clarkson, G. J.; van Gorkum, R.; Scott, P. *Chem. Commun.* **2009**, 1727.
(102) Sebli, C. P.; Howson, S. E.; Clarkson, G. J.; Scott, P. *Dalton Trans.* **2010**, *39*, 4447.